Journal of Power Sources 409 (2019) 24–30

Contents lists available at ScienceDirect

Journal of Power Sources

journal homepage: www.elsevier.com/locate/jpowsour

Graphite as a potassium ion battery anode in carbonate-based electrolyte and ether-based electrolyte

Liping Wang[a,b], Jingyi Yang[a], Jie Li[a], Ting Chen[b], Shulin Chen[c], Zhenrui Wu[a], Jiliang Qiu[d], Bojun Wang[a], Peng Gao[c,e,f,*], Xiaobin Niu[a,**], Hong Li[d]

[a] School of Materials and Energy, State Key Laboratory of Electronic Thin Film and Integrated Devices, University of Electronic Science and Technology of China, Chengdu, 610054, China
[b] State Key Laboratory of Advanced Chemical Power Sources, Guizhou Meiling Power Sources Co. Ltd, Zunyi, Guizhou, 563003, China
[c] International Center for Quantum Materials, School of Physics, Peking University, Beijing, 100871, China
[d] Institute of Physics, Chinese Academy of Sciences, Beijing, 100190, China
[e] Electron Microscopy Laboratory, School of Physics, Peking University, Beijing, 100871, China
[f] Collaborative Innovation Centre of Quantum Matter, Beijing, 100871, China

HIGHLIGHTS

- Graphite anode in ether-based electrolyte has good rate performance.
- Different thermodynamic operational voltages in different electrolytes.
- K^+-DME complexes co-insert into graphite.
- No formation of SEI between DME-based electrolyte and graphite.
- Low volume expansion and high K^+ diffusion rate in DME-based electrolyte.

GRAPHICAL ABSTRACT

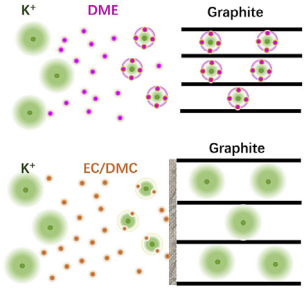

ARTICLE INFO

Keywords:
Potassium ion battery
Graphite
Ether-based electrolyte
Carbonate-based electrolyte
Solid electrolyte interphase

ABSTRACT

The graphite as the potassium ion battery anode is studied in KPF_6-EC/DMC and KPF_6-DME electrolytes. It is found that the graphite demonstrates superior rate performance with a capacity of 87 mAh g^{-1} at a current rate of 10 *C* (corresponding to 2.8 A g^{-1}) and excellent capacity retention ability of 84% after 3500 cycles in DME-based electrolyte. Moreover, its initial coulombic efficiency is 87.4%, higher than 69.6% in EC/DMC-based electrolyte. The K^+ solvating with DME complexes co-intercalate into graphite leading a high operational voltage at ~0.7 V vs. ~0.2 V in carbonate-based electrolyte, a fast apparent K^+ diffusion coefficient of 10^{-8} cm^2 s^{-1}, a negligible solid-electrolyte interface film, a small volume expansion (7.7% in (002) plane vs. 63% in EC/DMC electrolyte). This study addresses the importance of electrolyte in altering the potassium storage mechanisms to tune the energy density and power density in potassium ion batteries (KIBs).

1. Introduction

Lithium ion batteries (LIBs) with high energy density and power density are flagships in energy storage devices [1–4]. While the lithium as a trace mineral in earth's crust, mainly locating at Latin America, is only 20 ppm and it distributes unevenly in the global. Thus, other

* Corresponding author. International Center for Quantum Materials, School of Physics, Peking University, Beijing, 100871, China.
** Corresponding author.
E-mail addresses: pengg@pku.edu.cn (P. Gao), xbniu@uestc.edu.cn (X. Niu).

https://doi.org/10.1016/j.jpowsour.2018.10.092
Received 17 July 2018; Received in revised form 1 October 2018; Accepted 29 October 2018
Available online 03 November 2018
0378-7753/

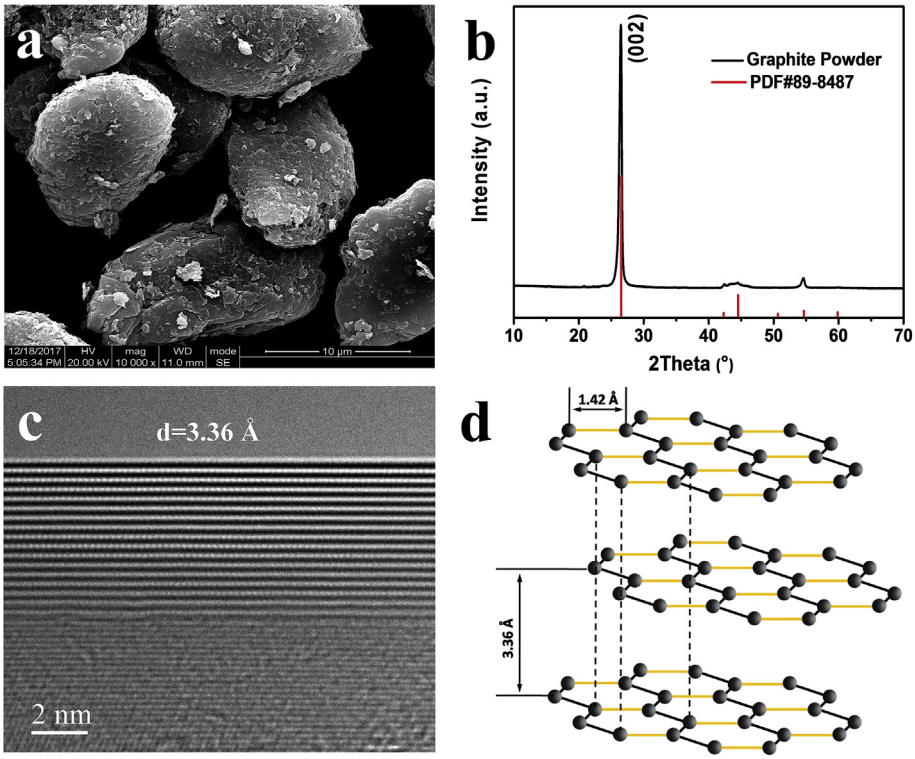

Fig. 1. Phase characterization and morphology of graphite. (a) SEM image, (b) XRD pattern, (c) HRTEM image, (d) Crystallographic structure.

alkaline metal ions, for instance, Na^+ and K^+, having similar chemical properties with Li^+ are alternatives. K element (2.6%) is one of the most natural common sources. The cost of potassium carbonate is 1/6 of lithium carbonate [5] and the electrolyte salt $LiPF_6$ costs about 20 times more than KPF_6 [6]. Moreover, the redox potential for K^+/K is −2.93 V vs. SHE, which is close to −3.04 V of Li^+/Li and lower than −2.71 V of Na^+/Na [7]. In addition, the Al has no electrochemical reactions with K so that Al can be used as the current collector at the anode side instead of Cu that is typically used in lithium ion batteries. In this way, the potassium ion batteries (KIBs) possibly offer higher energy densities than LIBs and sodium ion batteries (NIBs) in practical applications. Note that although the K^+ has a larger ionic radius 1.38 Å than 0.76 Å of Li^+ and 1.02 Å of Na^+, it has a lower Lewis acidity which leads to a smaller Stokes radius. For example, the Li^+, Na^+, and K^+ in propylene carbonate (PC) solvents have the Stokes radii 4.8 Å, 4.6 Å, and 3.6 Å, respectively [8]. Meanwhile, the potassium salt can have a higher ionic conductivity compared with lithium salt and sodium salt in PC solvent. A small Stokes radius and high ionic conductivity guarantee a high power density for KIBs.

Till now, a variety of electrodes have been reported for KIBs [7,9,10]. As for cathodes, Prussian blue analogues $K_2M[Fe(CN)_6]$ with M = Fe, Mn, Cu, Ni etc. [11,12], $KVOPO_4$, and $KVPO_4F$ [13] have demonstrated promising high operational voltages > 4.0 V vs. K^+/K. Regarding anodes, various carbons including hard carbon, soft carbon, graphene, and graphite have been reported [14–17]. Among them, graphite, which is one of the most common and the most successful commercial LIBs anodes, is reported to form KC_8 with a theoretical capacity of 280 mAh g^{-1} [15]. Compared with LiC_6, which has an expansion of 10% in the (002) plane from graphite [18], formation of KC_8 makes a huge linear expansion from 3.36 Å to 5.32 Å to be 58% [19], resulting in a poor capacity retention behavior. But it is still intriguing and surprising as graphite is assumed to have no ability of storage K since it is already reported that Na^+ can not insert into graphite in the same analogue type electrolyte [20].

It is known that electrolyte plays an important role on the electrochemical performance of electrodes, including capacity, rate performance, operational voltages, cycling performance, and so on [21]. Graphite demonstrates no capacity as sodium ion anodes in $NaPF_6$-PC electrolyte, but a capacity of 150 mAh g^{-1} with an operational voltage of 0.5 V in $NaPF_6$-DEGDME electrolyte [22]. In our recent study, we have found that TiS_2 as the KIBs cathode in carbonate-based electrolyte and ether-based electrolyte has a similar thermodynamic behavior, but totally different kinetic response [10]. The solvents have various electron donation numbers, which bring in “naked” or “sheath” ions and have influences on the interaction force with host electrode materials. Simultaneously, the solvents have different chemical and electrochemical stability leading solid electrolyte interphases (SEI) with distinct physico-chemical properties.

In this study, we revisit the graphite as a potassium ion batteries anode. We comparatively study its electrochemical properties including thermodynamic and kinetic behaviors in carbonate-based and ether-based electrolytes. Taking advantages of galvanostatic intermittent titration technique (GITT), Randle-Sevcik equation based on cyclic voltammetry (CV), electrochemical impedance spectroscopy (EIS) as well as transmission electron microscopy (TEM), it is found that the carbonate-based and ether-based electrolytes bring about different potassium atom storage behaviors in graphite in terms of operational voltage, capacity, as well as rate performance. K^+-DME complexes having small Stokes radii co-intercalate into graphite with a small volume swell (7%–15%), a fast diffusion rate ($\sim 10^{-8}$ cm^2 s^{-1}), and almost no formation of SEI with a high initial Coulombic efficiency 87%.

2. Experimental and characterizations

2.1. Electrode preparation and electrochemical tests

Graphite bought from Iopsilion Company was directly used without any modification or further treatment. Graphite electrodes were composed of the active material (nature graphite, 90 wt %), sodium carboxymethyl cellulose (CMC) binder (5 wt %) and Super P (5 wt %) on copper foil. They were dried in vacuum oven at 110 °C for 10 h before assembling. The average weight of the active material per graphite

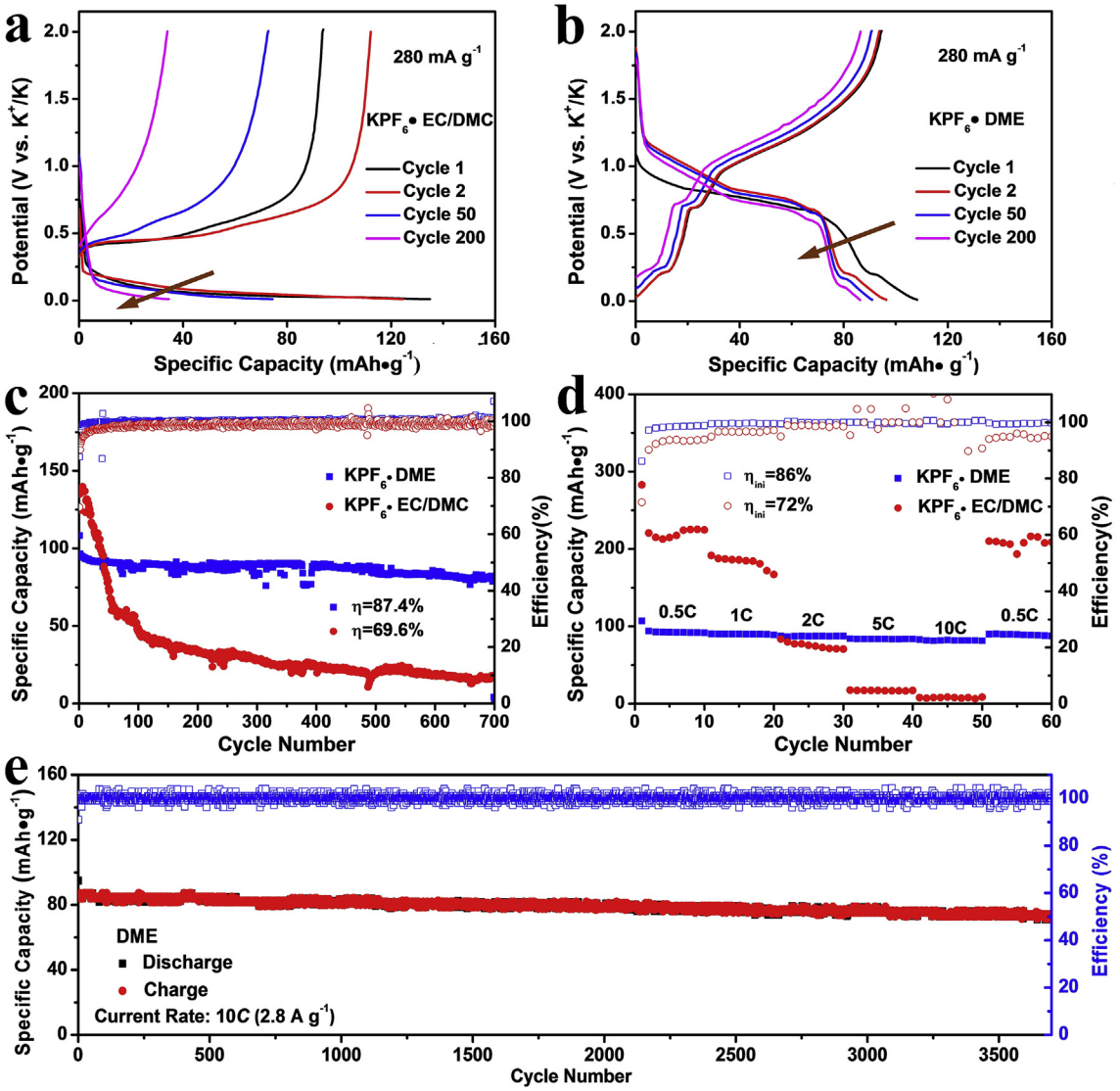

Fig. 2. Electrochemical performance of graphite. Galvanostatic discharge-charge curves (a) in carbonate-based electrolyte and (b) in ether-based electrolyte, (c) cycling performance, (d) rate performance, (e) high rate performance at 10 *C* in DME-based electrolyte.

electrode was about 2.0 mg cm^{-2}. Potassium metal and glass fiber film were used as the anode electrode and the separator, respectively. The electrolytes were 1M KPF_6 dissolved in 1,2-dimethoxyethane (DME, called ether-based electrolyte) and ethylene carbonate/dimethyl carbonate mixture (EC/DMC by 1:1 vol, called carbonate-based electrolyte). The half-cells were assembled in an argon-filled glove box. All the electrochemical tests are performed using a 2-electrode cell with graphite as a working electrode and potassium metal as a countering electrode. The electrochemical performance measurements were using a CT2001A cell test instrument (LANHE Electronic Co.) in the voltage range of 0.01–2.00 V. Cyclic voltammetry (CV) was tested using Arbin BT2000 electrochemical workstation (Arbin Instruments Co. Ltd.). Electrochemical impedance spectroscope (EIS) measurements were performed at the frequency range of 10 mHz- 10^5 Hz at amplitude of 10 mV. Galvanostatic intermittent titration technique (GITT) measurement were measured by using constant current density *C*/5 for 3 min then relaxing for 30 min (1 *C* corresponds to current density 280 mA g^{-1} to form KC_8).

2.2. Materials characterizations

Scanning Electron Microscopy (SEM) images were taken by Hitachi S-4800 (Japan). Transmission electron microscopy (TEM) was performed using an aberration-corrected FEI Titan Themis G2 microscope operated at 80 kV. X-ray diffraction (XRD) patterns were recorded by X'Pert ProMPD using CuKα radiation (λ = 1.5418 Å) with a scan step of 0.02° in the 2θ range of 10°–70°. Raman measurements were performed using OTBP1218-200 with a 532 nm laser source (ZOLIX INSTRUMENTS CO., LTD.).

3. Results and discussion

SEM image in Fig. 1a shows that the graphite has ellipsoidal shapes with sizes from 5 μm to 15 μm. The big micro-size particle is composed of nano-size plates. XRD pattern (Fig. 1b) demonstrates that the graphite is a pure hexagonal phase (S.G. P63 mc), which is well indexed to the JCPDS card No. 89–8487. According to the Bragg's law of λ = 2dsinθ, the lattice plane (002) located at 2θ = 26.49° has a layer distance of 3.36 Å. It is in line with the TEM observation (Fig. 1c). Its crystallographic structure is presented in Fig. 1d, which are ABA stacking graphene layers via Wan der Walls forces. Since the C—C is sp^2 covalent bonds in the hexagonal sheet, the p_z orbitals out of plane provides the electrons to form un-localized π bonds so as to have the metallic properties with a high electrical property of 10^3 S cm^{-1} in bulk

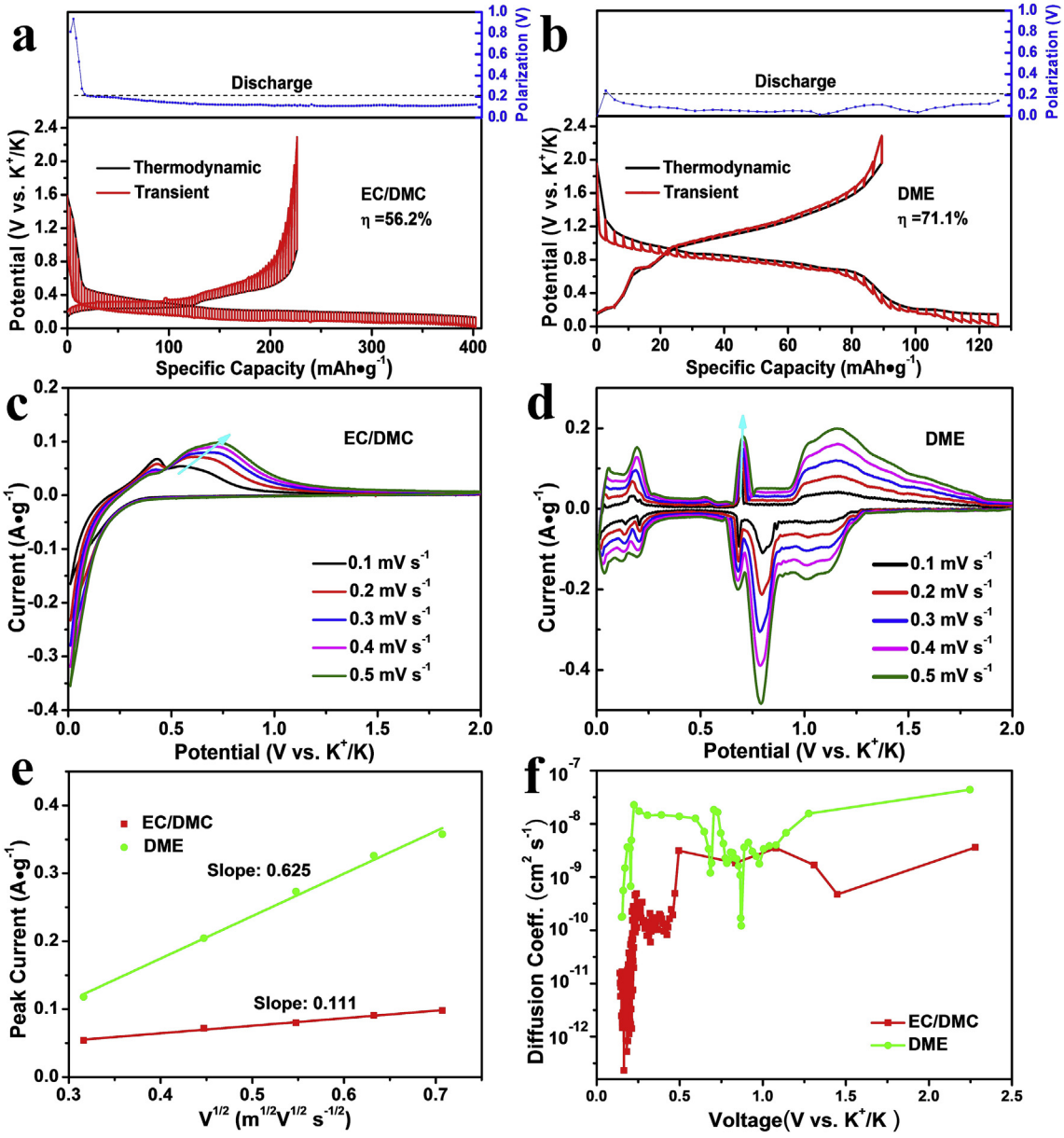

Fig. 3. GITT curves and voltage polarization in discharge process (a) in carbonate-based electrolyte and (b) in ether-based electrolyte, (c) cyclic voltammetry curves at different scan rates in EC/DMC system, (d) cyclic voltammetry curves at different scan rates in DME system, (e) The peak current as a function of square root of scan rate based on cyclic voltammetry curves, (f) K^+ diffusion coefficients at various voltages based on GITT curves.

[23].

The electrochemical performances of graphite as K-ion battery anodes in KPF_6-EC/DMC electrolyte and KPF_6-DME electrolyte are shown in Fig. 2. Galvanostatic discharge-charge curves depict that there is a high electrochemical polarization in carbonate-based electrolyte (Fig. 2a). Its initial discharge capacity is 135 mAh g^{-1} at a current density of 1 *C* (280 mA g^{-1}), far from the theoretical capacity of 280 mAh g^{-1}. Meanwhile, it suffers from severe capacity decay to be 125 mAh g^{-1}, 74 mAh g^{-1}, 34 mAh g^{-1} at the 2nd, 50th and 200th cycle, respectively. In contrast, the initial discharge capacity in DME-based electrolyte is a little low to be 108 mAh g^{-1} (Fig. 2b). However, it is 96 mAh g^{-1}, 91 mAh g^{-1}, 86 mAh g^{-1} at the 2nd, 50th and 200th cycle, respectively. The capacity decay rate is 0.1% per cycle on average. Kim et al. observed a similar capacity with ~100 mAh g^{-1} when sodium inserts into graphite in $NaPF_6$-DME electrolyte [24]. It is worth mentioning that the operational voltage in DME system is about 0.7 V vs. K^+/K, much higher than ~0.2 V in EC/DMC one. According to the report of Adelhelm and Kim et al., they have also obtained similar phenomena in Na storage natural graphite with $NaPF_6$-DEGDME electrolyte [22,25]. They ascribed to the formation of $[K\text{-}DME_y]^+$-graphite complex. Based on the Nernst equation ($\Delta_rG^\theta = -nFE^\theta$), the standard operational voltage is determined by the Gibbs free energy, which is effected by the energy between initial graphite and K-DME_yC_n complex.

The detailed capacity as a function of cycling number at 1 *C* rate is provided in Fig. 2c. It is obvious that the graphite in DME-based electrolyte has a much better capacity retention behavior with a capacity of 80 mAh g^{-1} after 700 cycles versus 17 mAh g^{-1} at 700th in EC/DMC-based one. Moreover, the initial Coulombic efficiency, an important parameter in the practical cell to match the cathode part for high energy density, is 87.4% in DME-based electrolyte versus 69.6% in EC/DMC system. It is also higher than the reported hard carbon (61.8%) [16] and soft carbon (56.4%) [15]. The DME-based electrolyte embodies its superiority to offer an outstanding rate performance as demonstrated in Fig. 2d. With the increase of current rate, the K storage

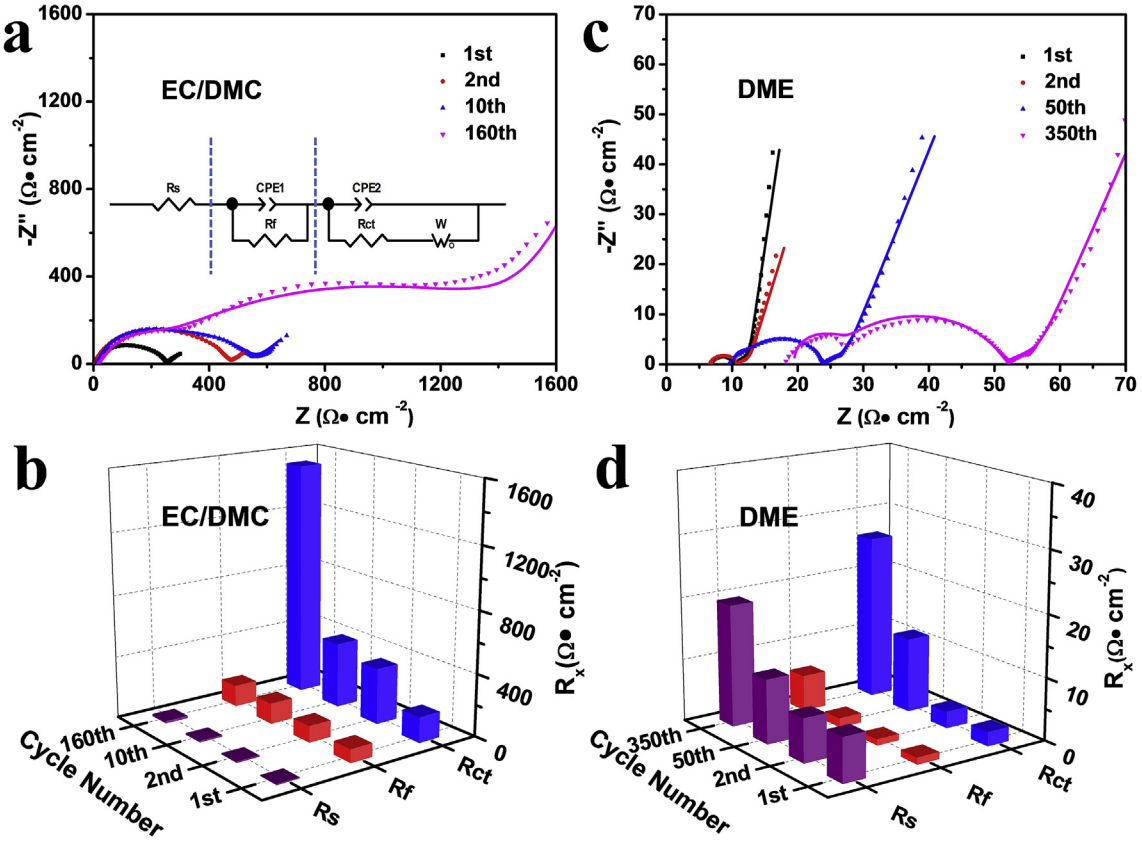

Fig. 4. Electrochemical impedance spectroscopy and fitting results for graphite at discharge state of 0.01 V in (a–b) EC/DMC-based electrolyte and (c–d) in DME-based electrolyte.

capacity is almost constant. It is 90 mAh g^{-1} at 0.5 *C* (140 mA g^{-1}) and 82 mAh g^{-1} at 10 *C* (2.8 A g^{-1}). While in the carbonate-based electrolyte, the graphite severely suffers from capacity loss from ~220 mAh g^{-1} at 0.5 *C* to 8 mAh g^{-1} at 10 *C*, which indicates that the performance is highly limited by kinetics. The graphite with DME-based electrolyte with initial discharge capacity of 94 mAh g^{-1} decreases to 50 mAh g^{-1} after 3800 cycles at 10 *C* (Fig. 2e). The rate performance is comparable with the Na behavior in ether-based system [17,22,26], and superior than other reports of graphite as KIBs anodes [14,27–29].

Galvanostatic intermittent titration technique (GITT) is employed to detect the thermodynamic operational voltage (Fig. 3a–b). Its polarization potentials ΔV are correspondingly determined. It is confirmed that the K is comparatively easier to intercalate into graphite in DME evidenced with a high operational voltage at ~0.7 V vs. K^+/K. As in the EC/DMC system, according to the equilibrium state curve (the black color) with a step-by-step plateau shape, which is a typical phase-to-phase transition mechanism, it is explored to be stage structures from KC_{36} to KC_{24}, then to KC_8 [15]. Nevertheless, the voltage-capacity curve in the DME-system is much more complicated with both a phase-to-phase transition at ~0.7 V and a solid-solution behavior above 0.7 V. Overall, the potential polarization ΔV in DME-based electrolyte is less than 0.2 V, smaller than that in EC/DMC-based one. CV curves at different scan rates obey the Randles-Sevcik relation (Fig. 3c–e), meaning the K ion diffusion in the solid-state electrode is the rate-determined step [30,31]. The peak current density as a function of the square root of the scan rate with a higher slop in the DME-based electrolyte testifies a better kinetic behavior. According to the Randles-Sevcik equation [32] $I_P = 0.4463n^{3/2}F^{3/2}C_{K^+}SR^{-1/2}T^{-1/2}D^{1/2}v^{1/2}$, where I_p is the peak current (A), n is the number of electron transferred for the specific redox couple (assuming formation of KC_8, n = 1/8), F is the Faraday constant (96485.4 C mol^{-1}), C is the potassium ion concentration in graphite (0.0234 mol cm^{-3}), S is the electrode area (1.13 cm^2), R is the gas constant (8.314 J mol^{-1} K^{-1}), T is the temperature (298 K), D the diffusion coefficient (cm^2 s^{-1}), v is the scanning rate (V s^{-1}), we obtain the K^+ diffusion coefficients 6.1×10^{-10} cm^2 s^{-1} in EC/DMC-type system and 3.0×10^{-8} cm^2 s^{-1} in DME-type system. Meanwhile, we have also calculated the K^+ diffusion coefficient based on the GITT results using the equation [16]:

$$D_{K^+} = \frac{4}{\pi}\left(\frac{m_B V_M}{M_B S}\right)^2\left(\frac{\Delta E_S}{\tau(dE_\tau/d\sqrt{\tau})}\right)^2 \approx \frac{4}{\pi\tau}\left(\frac{m_B V_M}{M_B S}\right)^2\left(\frac{\Delta E_S}{\Delta E_\tau}\right)^2 \quad (\tau \ll L^2/D_{K^+})$$

Where m_B is the mass (0.0024 g in our case), m_B is the molecular weight of graphite (12.01 g mol^{-1}), V_M is the molar volume of graphite (42.74 cm^3 mol^{-1}), S is the effective area of the electrode (1.13 cm^2), $dE\tau/d\sqrt{\tau}$ is the slope of the linearized proportional of the E_τ during the potassiation or depotassiation process of duration time τ(s), △Es is the potential change after every equilibrium process, L is the thickness of the electrodes. We have obtained the K^+ diffusion coefficients ~10^{-10} cm^2 s^{-1} in EC/DMC-type system and 5.0×10^{-8} cm^2 s^{-1} in DME-type system, as shown in Fig. 3f. The diffusion coefficient in EC/DMC is next to that of hard carbon [16] and comparable with the Li^+ rate insertion into graphite [33]. The high K^+ diffusion coefficient in DME-type electrolyte hints that the potassium ion batteries can afford high rate performance in optimal electrolyte system.

Electrochemical impedance spectroscopy (EIS) at the discharge state is introduced to explore the effect of electrolytes on electrochemical property differences (Fig. 4a–b). The equivalent circuit (inset, Fig. 4a) consisting of internal resistance (R_s), SEI resistance (R_f), and charge transfer resistance (R_{ct}) is used to fit the EIS (Fig. 4c–d). At the beginning, the overall resistance (R_s + R_f + R_{ct}) in the EC/DMC-based electrolyte cell is two orders of magnitude higher (~251 Ω) than 10 Ω of DME-based one. The R_{ct} in EC/DMC-based increases rapidly from

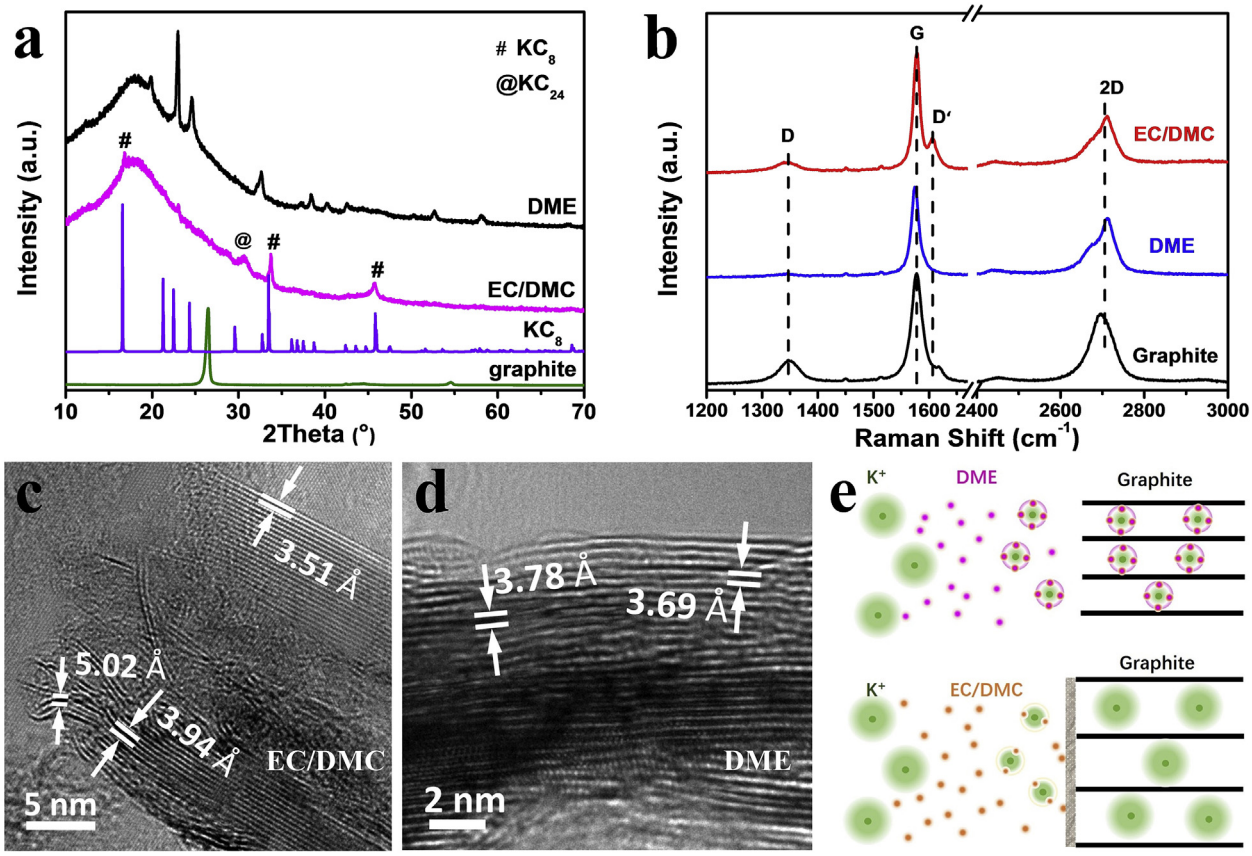

Fig. 5. (a) XRD patterns at the discharge state 0.01 V, (b) Raman spectra of graphite at discharge voltage 0.01 V, TEM images of discharged graphite (c) in EC/DMC electrolyte and (d) in DME electrolyte, (e) Schematic illustration for graphite response in different electrolytes.

162 Ω at the 1st cycle to 1520 Ω at the 160th cycle. Such a dramatic increase means a quick loss of electrochemical active sites in graphite, which might be related with huge volume expansion and irreversible K atoms accumulating. On the other hand, there is almost no formation of SEI in DME cell since the R_f is less than 10 Ω even after 350 cycles (vs. ~200 Ω in EC/DMC cell). The absence of SEI can favorably furnish a high diffusion rate as evidenced in Fig. 3d.

The K storage mechanism in phase structures is detected via XRD patterns and Raman spectroscopy (Fig. 5a–b). Identical with Zhao's report [18], KC_8 and KC_{24} are formed in the discharged state in EC/DMC-based electrolyte. Based on the characteristic peak at 2theta = 16.8°, the (002) lattice plane expands 63% from pristine 3.36 Å to 5.49 Å. It is huge compared with the reported $KVPO_4F$ with volume shrinkage 5.8% and 3.3% for $KVOPO_4$ [13]. Such an expansion is difficult to recover and make the electrode loss contact for a big charge-transfer resistance. Meanwhile, the behavior of K storage in the graphite in DME-based electrolyte is totally distinct as they share no diffraction peaks in the XRD pattern. The characteristic peaks at 2theta 24.6° and 22.3° reveal lattice distances to be 3.62 Å (7.1%) and 3.86 Å (14.9%), respectively. A small volume change renders a good capacity retention behavior. At the discharge state, the intensity ratio I_D/I_G in carbonate-based electrolyte is 0.088, larger than 0.035 in DME-based electrolyte, indicating an increase defects in the sp^3-defects, which is well consistent with the huge volume change as evidenced in XRD results [34]. High resolution TEM image (Fig. 5c) at the discharged state confirms that the graphite in EC/DMC-based electrolyte has a huge volume expansion with distortion to be 5.02 Å, 3.94 Å, and 3.51 Å. In contrast, demonstrated in Fig. 5d, the K inserted graphite in ether electrolyte has a relatively well-ordered structure with lattice spacing 3.69 Å −3.78 Å. A small volume expansion can well explain its good cycling performance and low charge transfer resistance. Meanwhile, loose porous SEI is observed on the graphite surface in carbonate electrolyte while the graphite fringe in ether electrolyte is smooth. A schematic illustration (Fig. 5e) is displayed to interpret the distinct electrochemical response of graphite in different electrolytes pertaining to operational voltage and power rate. DME electrolyte has a larger electron donation number 20 than 16 of EC [35,36] so that it has a higher binding energy with K^+ to form K^+-DME complexes. The complexes with "sheath" co-intercalate into the graphite. Simultaneously, the LUMO level of K^+-DME solvent would be higher than graphite so that they have no electrochemical reactions to form SEI [20]. In words, the [K-solvent]$^+$ molecular insert into graphite without SEI blockage to form thermodynamic stable phases concomitantly with small volume expansions.

4. Conclusions

The electrochemical performances of graphite as a potassium ion battery anode are comparatively studied in carbonate-based and ether-based electrolytes. Graphite in DME-based electrolytes offers a high operational voltage at ~0.7 V (versus 0.2 V in EC/DMC-based one), good rate performance with 80 mAh g^{-1} at 10 *C* with a negligible solid electrolyte interface, and a small volume expansion (3.36 Å to 3.62 Å for (002) plane). Different from the K^+ intercalation into graphite with formation of KC_8 in EC/DMC-based electrolyte, the K^+-ether co-intercalates into the graphite, which presumably has a charge shielding effect with a consequence of low interaction force with graphite leading a high insertion voltage, high apparent K^+ diffusion rate 10^{-8} cm^2 s^{-1} and low volume expansion (< 10%). This study demonstrates the importance of optimizing electrolytes to improve the electrodes' energy density and power density.

Acknowledgments

This work is supported by the National Natural Science Foundation of China (51502032, 51502007, 51672007), National Key Research and Development Program of China (Grant no. 2018YFA0306100), the Fundamental Research Funds for the Central Universities, China (No. ZYGX2016J044), and the Opening Project of State Key Laboratory of Advanced Chemical Power Sources (SKL-ACPS-C-12). We gratefully acknowledge Electron Microscopy Laboratory in Peking University for the use of Cs corrected electron microscope.

References

[1] M. Hu, X. Pang, Z. Zhou, Review recent progress in high-voltage lithium ion batteries, J. Power Sources 237 (2013) 229–242.
[2] L. Wang, Q. Wang, W. Jia, S. Chen, P. Gao, J. Li, Li metal coated with amorphous Li_3PO_4 via magnetron sputtering for stable and long-cycle life lithium metal batteries, J. Power Sources 342 (2017) 175–182.
[3] L. Wang, H. Li, X. Huang, E. Baudrin, A comparative study of Fd-3m and $P4_332$ "$LiNi_{0.5}Mn_{1.5}O_4$", Solid State Ionics 193 (2011) 32–38.
[4] Y. Liu, L. Wang, L. Cao, C. Shang, Z. Wang, H. Wang, L. He, J. Yang, H. Cheng, J. Li, Understanding and suppressing side reactions in Li-air batteries, Mater. Chem. Front. 1 (2017) 2495–2510.
[5] H. Kim, J.C. Kim, M. Bianchini, D.H. Seo, J. Rodriguez-Garcia, G. Ceder, Recent progress and perspective in electrode materials for K-ion batteries, Adv. Energy Mater. 8 (2018) 1702384.
[6] J.C. Pramudita, D. Sehrawat, D. Goonetilleke, N. Sharma, An initial review of the status of electrode materials for potassium-ion batteries, Adv. Energy Mater. 7 (2017) 1602911.
[7] K. Kubota, M. Dahbi, T. Hosaka, S. Kumakura, S. Komaba, Towards K-ion and Na-ion batteries as "Beyond Li-ion", Chem. Rec. 18 (2018) 459–479.
[8] Y. Matsuda, H. Nakashima, M. Morita, Y. Takasu, Behavior of some ions in mixed organic electrolytes of high energy density batteries, J. Electrochem. Soc. 128 (1981) 2552–2556.
[9] A. Eftekhari, Z. Jian, X. Ji, Potassium secondary batteries, ACS Appl. Mater. Interfaces 9 (2016) 4404–4419.
[10] L. Wang, J. Zou, S. Chen, G. Zhou, J. Bai, P. Gao, Y. Wang, X. Yu, J. Li, Y. Hu, TiS_2 as a high performance potassium ion battery cathode in ether-based electrolyte, Energy Storage Mater. 12 (2018) 216–222.
[11] L. Xue, Y. Li, H. Gao, W. Zhou, X. Lü, W. Kaveevivitchai, A. Manthiram, J.B. Goodenough, Low-cost high-energy potassium cathode, J. Am. Chem. Soc. 139 (2017) 2164–2167.
[12] X. Bie, K. Kubota, T. Hosaka, K. Chihara, S. Komaba, A novel K-ion battery: hexacyanoferrate (II)/graphite cell, J. Mater. Chem. A 5 (2017) 4325–4330.
[13] K. Chihara, A. Katogi, K. Kubota, S. Komaba, $KVPO_4F$ and $KVOPO_4$ toward 4 volt-class potassium-ion batteries, Chem. Commun. 53 (2017) 5208–5211.
[14] S. Komaba, T. Hasegawa, M. Dahbi, K. Kubota, Potassium intercalation into graphite to realize high-voltage/high-power potassium-ion batteries and potassium-ion capacitors, Electrochem. Commun. 60 (2015) 172–175.
[15] Z. Jian, W. Luo, X. Ji, Carbon electrodes for K-ion batteries, J. Am. Chem. Soc. 137 (2015) 11566–11569.
[16] Z. Jian, Z. Xing, C. Bommier, Z. Li, X. Ji, Hard carbon microspheres: potassium-ion anode versus sodium-ion anode, Adv. Energy Mater. 6 (2016) 1501874.
[17] C. Chen, Z. Wang, B. Zhang, L. Miao, J. Cai, L. Peng, Y. Huang, J. Jiang, Y. Huang, L. Zhang, Nitrogen-rich hard carbon as a highly durable anode for high-power potassium-ion batteries, Energy Storage Mater. 8 (2017) 161–168.
[18] J. Zhao, X. Zou, Y. Zhu, Y. Xu, C. Wang, Electrochemical intercalation of potassium into graphite, Adv. Funct. Mater. 26 (2016) 8103–8110.
[19] R. Tossici, M. Berrettoni, M. Rosolen, R. Marassi, B. Scrosati, Electrochemistry of KC_8 in lithium-containing electrolytes and its use in lithium-ion cells, J. Electrochem. Soc. 144 (1997) 186–192.
[20] G. Yoon, H. Kim, I. Park, K. Kang, Conditions for reversible Na intercalation in graphite: theoretical studies on the interplay among guest ions, solvent, and graphite host, Adv. Energy Mater. 7 (2017) 1601519.
[21] H. Pan, J. Chen, R. Cao, V. Murugesan, N.N. Rajput, K.S. Han, K. Persson, L. Estevez, M.H. Engelhard, J. Zhang, Non-encapsulation approach for high-performance Li-S batteries through controlled nucleation and growth, Nat. Energy 2 (2017) 813–820.
[22] H. Kim, J. Hong, Y.U. Park, J. Kim, I. Hwang, K. Kang, Sodium storage behavior in natural graphite using ether-based electrolyte systems, Adv. Funct. Mater. 25 (2015) 534–541.
[23] A.G. Pandolfo, A.F. Hollenkamp, Carbon properties and their role in supercapacitors, J. Power Sources 157 (2006) 11–27.
[24] H. Kim, J. Hong, G. Yoon, H. Kim, K.Y. Park, M.S. Park, W.S. Yoon, K. Kang, Sodium intercalation chemistry in graphite, Energy Environ. Sci. 8 (2015) 2963–2969.
[25] B. Jache, P. Adelhelm, Use of graphite as a highly reversible electrode with superior cycle life for sodium-ion batteries by making use of co-intercalation phenomena, Angew. Chem. Int. Ed. 53 (2014) 10169–10173.
[26] R.A. Adams, J.M. Syu, Y. Zhao, C.T. Lo, A. Varma, V.G. Pol, Binder-free N-and O-rich carbon nanofiber anodes for long cycle life K-ion batteries, ACS Appl. Mater. Interfaces 9 (2017) 17872–17881.
[27] Y. Xie, Y. Chen, L. Liu, P. Tao, M. Fan, N. Xu, X. Shen, C. Yan, Ultra-high pyridinic N-doped porous carbon monolith enabling high-capacity K-ion battery anodes for both half-cell and full-cell applications, Adv. Mater. 29 (2017) 1702268.
[28] W. Luo, J. Wan, B. Ozdemir, W. Bao, Y. Chen, J. Dai, H. Lin, Y. Xu, F. Gu, V. Barone, Potassium ion batteries with graphitic materials, Nano Lett. 15 (2015) 7671–7677.
[29] A.P. Cohn, N. Muralidharan, R. Carter, K. Share, L. Oakes, C.L. Pint, Durable potassium ion battery electrodes from high-rate cointercalation into graphitic carbons, J. Mater. Chem. A 4 (2016) 14954–14959.
[30] X. Dai, L. Wang, J. Xu, Y. Wang, A. Zhou, J. Li, Improved electrochemical performance of $LiCoO_2$ electrodes with ZnO coating by radio frequency magnetron sputtering, ACS Appl. Mater. Interfaces 6 (2014) 15853–15859.
[31] L. Wang, J. Bai, P. Gao, X. Wang, J.P. Looney, F. Wang, Structure tracking aided design and synthesis of $Li_3V_2(PO_4)_3$ nanocrystals as high-power cathodes for lithium ion batteries, Chem. Mater. 27 (2015) 5712–5718.
[32] L. Wang, J. Xu, C. Wang, X. Cui, J. Li, Y. Zhou, A better understanding of the capacity fading mechanisms of $Li_3V_2(PO_4)_3$, RSC Adv. 5 (2015) 71684–71691.
[33] M.D. Levi, D. Aurbach, Diffusion coefficients of lithium ions during intercalation into graphite derived from the simultaneous measurements and modeling of electrochemical impedance and potentiostatic intermittent titration characteristics of thin graphite electrodes, J. Phys. Chem. B 101 (1997) 4641–4647.
[34] A. Eckmann, A. Felten, A. Mishchenko, L. Britnell, R. Krupke, K.S. Novoselov, C. Casiraghi, Probing the nature of defects in graphene by Raman spectroscopy, Nano Lett. 12 (2012) 3925–3930.
[35] H.D. Lim, B. Lee, Y. Bae, H. Park, Y. Ko, H. Kim, J. Kim, K. Kang, Reaction chemistry in rechargeable Li-O_2 batteries, Chem. Soc. Rev. 46 (2017) 2873–2888.
[36] D.M. Kim, S.C. Jung, S. Ha, Y. Kim, Y. Park, J.H. Ryu, Y.K. Han, K.T. Lee, Cointercalation of Mg^{2+} ions into graphite for magnesium-ion batteries, Chem. Mater. 30 (2018) 3199–3203.